ACS Catalysis

pubs.acs.org/acscatalysis Research Article

Indole Diketopiperazine Dimerization Catalyzed by Dye-Decolorizing Peroxidases via Hydroxyl-to-Carbon Radical Relay

Peng Fang, Wei Wang, Shuai Mu, Fei Guo, Xinwei Song, Xiang Sheng,* Lei Du,* and Shengying Li*

Cite This: https://doi.org/10.1021/acscatal.6c03866 Read Online

ACCESS | Metrics & More | Article Recommendations | Supporting Information

ABSTRACT: Indole diketopiperazine (DKP) alkaloids constitute an important class of fungal natural products with diverse biological activities. Although dimeric indole DKPs have been isolated from natural sources and often exhibit enhanced bioactivities compared with their monomeric counterparts, enzymatic dimerization of indole DKPs remains rare and mechanistically poorly understood. Here, we investigate the enzymatic dimerization of 6-hydroxy-deoxybrevianamide E (6-OH-DoE), an indole DKP intermediate selected based on reports of naturally occurring dimeric derivatives. In vitro assays revealed that dye-decolorizing peroxidases (DyPs) catalyze the regioselective dimerization of 6-OH-DoE, affording di-6-OH-DoE through exclusive C7–C7′ coupling on the indole moiety. Combined experimental and computational analyses indicate that the reaction proceeds through a hydroxyl-to-carbon radical relay pathway, initiated by oxidation of the indole hydroxyl group, followed by intramolecular radical transfer to the C7 position, rather than direct C–H hydrogen-atom abstraction. This mechanistic proposal was further validated by substrate analogue studies and radical-probing experiments. Furthermore, a homologous DyP enzyme from the native producer was shown to catalyze the same transformation. Collectively, this study elucidates the enzymatic mechanism of indole DKP dimerization and expands the catalytic repertoire of DyP peroxidases, highlighting their potential as biocatalysts for regioselective radical-mediated C–C bond formation in indole DKP scaffolds.

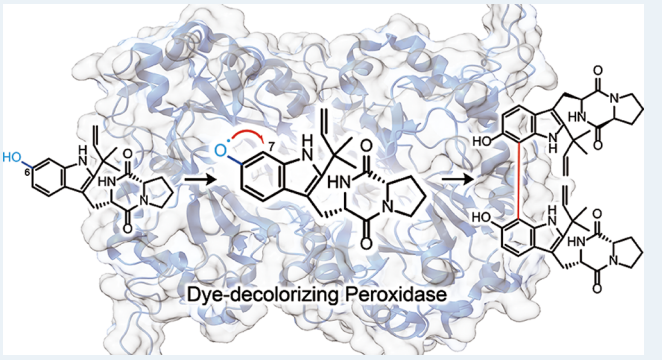

KEYWORDS: *indole diketopiperazine alkaloids, enzymatic dimerization, dye-decolorizing peroxidases, radical-mediated C–C coupling, biosynthesis*

INTRODUCTION

Indole diketopiperazine (DKP) alkaloids are a prominent class of fungal secondary metabolites featuring the fusion of indole and DKP scaffolds. These compounds are widely distributed in filamentous fungi, including *Aspergillus*, *Penicillium*, and *Chaetomium* species, and have attracted growing interest owing to their structural diversity, broad biological relevance, and pharmaceutical potential.[1−6] Representative members such as brevianamides, notoamides, and tryprostatins exemplify indole DKPs as privileged molecular frameworks in chemical biology and natural product research.[7−12]

Although the majority of indole DKPs occur as monomeric natural products, dimeric derivatives have also been isolated from natural sources and often display enhanced or distinct biological activities compared with their monomeric counterparts. Representative dimeric indole DKPs, such as dinotoamide J and stephacidin B, as well as structurally diverse dimeric natural products including neosartorin and gossypol, illustrate how dimerization can profoundly influence molecular function (Figure 1).[13−16] By combining two pharmacophores into a single molecular entity, dimerization can effectively modulate target engagement, signaling behavior, and physicochemical properties. Consistent with this notion, several studies have demonstrated that dimerization may dramatically enhance biological potency, in some cases by several orders of magnitude, underscoring dimer formation as a powerful strategy for natural product optimization.[17−20]

Despite the growing number of studies reporting dimeric products,[21−24] the enzymatic mechanisms underlying diverse dimerization reactions remain largely underexplored. This knowledge gap is particularly evident for indole DKP alkaloids, for which mechanistic studies of enzymatic C–C bond-forming dimerization are scarce.[25,26]

Received: May 18, 2026
Revised: July 14, 2026
Accepted: August 7, 2026

Downloaded from pubs.acs.org/acscatal/article-pdf/doi/10.1021/acscatal.6c03866/6740955O/cs-2026-03866s.pdf?guestAccessKey=b21ef2db-9291-4e47-bb75-c7f3cdbad6a by guest on 26 August 2026

© XXXX American Chemical Society

https://doi.org/10.1021/acscatal.6c03866
ACS Catal. XXXX, XXX, XXX−XXX

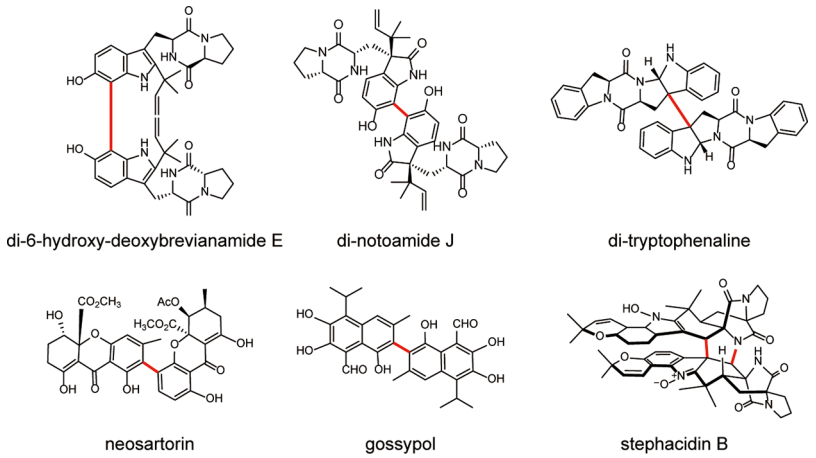

Figure 1. Representative dimeric natural products with the coupling bonds highlighted in red.

Among the reported indole DKP monomer–dimer pairs, 6-hydroxy-deoxybrevianamide E (6-OH-DoE) was selected in this study as a representative substrate for investigating enzymatic dimerization (Figure 1).[13] Its naturally occurring dimeric derivative suggests that 6-OH-DoE may serve as a biosynthetically relevant precursor for dimer formation. However, the enzyme responsible for this transformation and the molecular basis governing its regioselectivity and reactivity have not been elucidated. Consequently, a systematic study of 6-OH-DoE dimerization offers a unique opportunity to gain mechanistic insight into indole DKP dimer formation.

In this study, we investigated the enzymatic dimerization of 6-OH-DoE as a model system to understand the molecular mechanism of indole DKP dimerization. To access sufficient quantities of this key substrate, a heterologous biosynthetic pathway was constructed in *Aspergillus oryzae* M-2-3 (*Ao*)[27] for the targeted production of 6-OH-DoE. Through in vitro screening of diverse oxidoreductases, we identified dye-decolorizing peroxidases (DyPs) as effective catalysts for the regioselective dimerization of 6-OH-DoE. By integrating structural elucidation, quantum chemical calculations, substrate scope studies, and radical trapping experiments, we proposed a hydroxyl-to-carbon radical relay mechanism governing this transformation. This work provides mechanistic insight into indole DKP dimerization and underscores the utility of peroxidase-mediated radical coupling for tailoring indole DKP scaffolds.

RESULTS AND DISCUSSION

Targeted Production of 6-OH-DoE by Heterologous Biosynthesis

To enable a biochemical investigation of indole DKP dimerization, sufficient quantities of the biosynthetically relevant monomer substrate are required. Based on prior reports of naturally occurring dimeric derivatives, we selected 6-OH-DoE as the model substrate for this study.[13] A heterologous biosynthetic pathway was therefore constructed in *Ao*, a genetically tractable fungal host commonly used for the heterologous expression of fungal natural product biosynthetic pathways,[28] to enable the targeted production of 6-OH-DoE based on the previously known biosynthetic route of notoamide-type indole DKP alkaloids (Figure 2a).[29] Using L-tryptophan and L-proline as starting materials, the nonribosomal peptide synthetase NotE catalyzes the formation of brevianamide F, which is subsequently prenylated by the reverse prenyltransferase NotF to afford deoxybrevianamide E (DoE). Hydroxylation at the C6 position of the indole moiety is then mediated by the

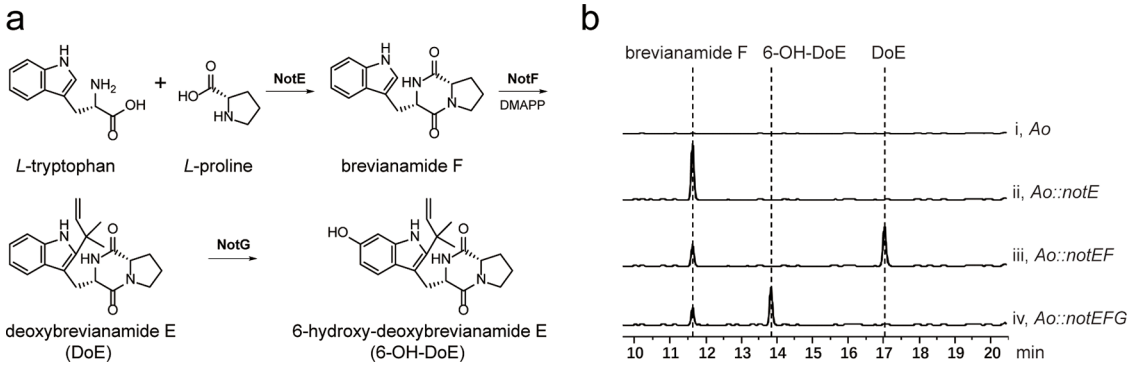

Figure 2. Heterologous biosynthesis of 6-OH-DoE. (a) Reconstructed biosynthetic route leading to 6-OH-DoE, based on the reported notoamide biosynthetic pathway. (b) HPLC analysis of *Ao* transformants expressing sequential combinations of notoamide biosynthetic genes, illustrating stepwise production of brevianamide F, deoxybrevianamide E, and 6-OH-DoE.

https://doi.org/10.1021/acscatal.6c03866
ACS Catal. XXXX, XXX, XXX–XXX

Downloaded from pubs.acs.org/acscatal/article-pdf/doi/10.1021/acscatal.6c03866/6740955O/cs-2026-03866s.pdf?guestAccessKey=b21cf2db-9291-4e47-bb75-c7f3ccfbad6a by guest on 26 August 2026

cytochrome P450 monooxygenase NotG, yielding 6-OH-DoE as the end product.

Expression of *NotE* alone led to the production of brevianamide F, giving a dominant peak (11.6 min) (Figure 2b, trace ii), consistent with NotE-catalyzed cyclodipeptide formation from L-tryptophan and L-proline. Co-expression of *NotE* and *NotF* resulted in the emergence of a new peak (17.0 min) (Figure 2b, trace iii), corresponding to DoE formed via reverse prenylation of brevianamide F by NotF. Upon further introduction of *NotG*, an additional peak appeared (13.8 min) (Figure 2b, trace iv), which was assigned as 6-OH-DoE, indicating efficient C6 hydroxylation of the indole moiety catalyzed by the cytochrome P450 monooxygenase NotG.

The target compound, 6-OH-DoE, together with the pathway intermediates brevianamide F and DoE, was purified from the corresponding fermentation extracts by semi-preparative HPLC. The structures of all three compounds were unambiguously confirmed by high-resolution mass spectrometry (Figure S1) and comprehensive NMR spectroscopic analyses (Figures S2–S7). These results validated the successful heterologous reconstruction of the targeted biosynthetic sequence and furnished well-characterized substrates for subsequent enzymatic dimerization and mechanistic investigations.

Identification of DyP-Type Peroxidases as Catalysts for 6-OH-DoE Dimerization

Oxidoreductases such as laccases, peroxygenases, and peroxidases are well known for their broad substrate scope and catalytic promiscuity. These enzymes can promote oxidative transformations involving one-electron oxidation and substrate-radical formation, including C–C bond formation, oxidative cross-coupling, and substrate oligomerization or polymerization.[30−34] On this basis, we reasoned that the dimerization of 6-OH-DoE could be mediated by a promiscuous oxidative enzyme capable of promoting oxidative coupling reactions. Of note, previous functional characterization of the notoamide biosynthetic genes has not revealed any plausible cluster-encoded enzymes that could account for dimerization of indole DKP intermediates.[29,35−37] Taken together, we hypothesized that the dimerization of 6-OH-DoE is most likely catalyzed by a cluster-independent oxidoreductase.

To test this hypothesis, a panel of versatile oxidoreductases with documented oxidative and coupling activities was selected for in vitro reaction screening. The enzyme set included a laccase from *Rhus verniciflua*,[38] an aromatic peroxygenase from *Cyclocybe aegerita* (Jed),[39] a vanadium-dependent chloroperoxidase from *Curvularia inaequalis* (VCPO),[40] horseradish peroxidase from *Armoracia rusticana* (HRP),[41] and four DyPs from *Bacillus subtilis* (Bsu-DyP),[42] *Corynebacterium glutamicum* (Cgl-DyP),[43] *Pseudomonas aeruginosa* (Pae-DyP),[44] and *Rhodococcus jostii* (DypB)[45] (Figure 3a). Except for the laccase and HRP, which were obtained commercially, VCPO and all DyPs were heterologously expressed in *Escherichia coli* BL21(DE3), while Jed was produced via secretory expression in *Pichia pastoris* GS115. All selected enzymes were obtained in soluble form and subjected to in vitro assays using 6-OH-DoE as the substrate.

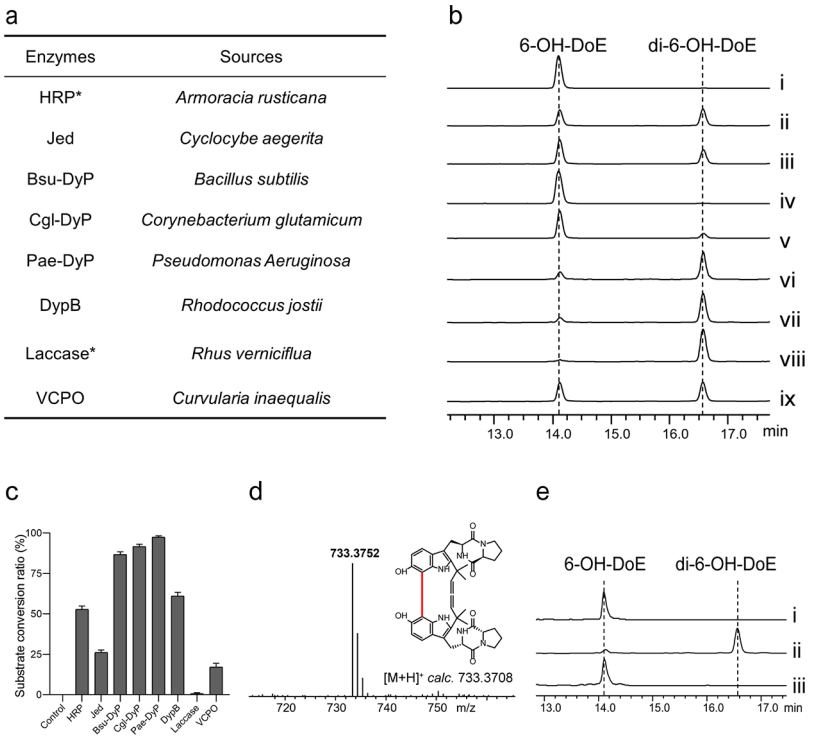

Figure 3. Identification of oxidoreductases capable of catalyzing oxidative transformation of 6-OH-DoE. (a) Sources of the candidate oxidoreductases evaluated in this study. Enzymes marked with an asterisk (*) were obtained commercially. (b) HPLC analysis of enzymatic reactions using 6-OH-DoE as the substrate. Reaction conditions: 1 mM substrate, 10 μM enzyme, and 2 mM H_2O_2 in 100 mM potassium phosphate buffer (pH 7.0), incubated at 30 °C for 2.5 h. (i) Heat-inactivated enzyme control; (ii) HRP; (iii) Jed; (iv) laccase; (v) VCPO; (vi) Bsu-DyP; (vii) Cgl-DyP; (viii) Pae-DyP; and (ix) DypB. (c) Comparison of substrate conversion efficiencies of 6-OH-DoE catalyzed by different oxidoreductases. Data are presented as mean ± SD ($n = 3$ independent experiments). (d) LC-MS analysis of the enzymatic reaction product. (e) HPLC analysis of enzymatic reactions catalyzed by endogenous enzymes. (i) Heat-inactivated enzyme control; (ii) DyP2566; and (iii) peroxidase-5153.

Downloaded from pubs.acs.org/acscatsc/article-pdf/doi/10.1021/acscatal.6c03866/6740955/cs-2026-03866s.pdf?guestAccessKey=b21ef2db-9291-4e47-bb75-c7f3cfbad6a by guest on 26 August 2026

https://doi.org/10.1021/acscatal.6c03866
ACS Catal. XXXX, XXX, XXX−XXX

HPLC analysis of the reaction mixtures revealed pronounced differences in catalytic performance among the tested oxidoreductases toward 6-OH-DoE. The results showed that DyP-type peroxidases were clearly capable of efficiently transforming 6-OH-DoE and exhibited the highest catalytic activity among the tested enzymes, with Pae-DyP providing the highest conversion under the testing conditions (Figure 3b, traces vi, vii, and viii; Figure 3c). The reactions catalyzed by DyPs reproducibly afforded a distinct product peak (16.6 min) that was absent in the corresponding control reactions, and all catalytically active DyPs generated the same product with an identical retention time, indicating a highly conserved and regioselective transformation. In comparison, HRP and the aromatic peroxygenase Jed displayed moderate activity toward 6-OH-DoE, producing the same product peak but at substantially lower levels (Figure 3b, traces ii and iii). By contrast, VCPO showed only marginal catalytic activity (Figure 3b, trace v), while the laccase exhibited little to undetectable conversion of 6-OH-DoE under the same conditions (Figure 3b, trace iv).

To enable further structural elucidation of the enzymatic reaction product, Pae-DyP—exhibiting the highest catalytic efficiency among the tested oxidoreductases—was selected as the model enzyme for subsequent preparative-scale reactions. LC–MS analysis of the DyP-catalyzed product revealed a molecular ion consistent with a dimer of 6-OH-DoE (Figure 3d). Preparative in vitro reactions using Pae-DyP afforded sufficient materials for comprehensive NMR characterization, and detailed ^{1}H and ^{13}C NMR analyses, together with comparison with previously reported spectroscopic data,[13] unambiguously established the product as a C7–C7′-linked dimer of 6-OH-DoE (Figures S8 and S9).

Notably, extensive functional and biosynthetic studies of the notoamide gene cluster have not identified any cluster-encoded enzymes capable of catalyzing dimerization reactions, indicating that this transformation is unlikely to be mediated by a pathway enzyme. To assess whether an off-cluster oxidoreductase encoded by the native producer accounts for this reaction, we examined the *Aspergillus versicolor* NRRL 35600 (*Aver221*) genome-derived proteome for potential candidates. Separate BLAST searches against this proteome retrieved two peroxidase proteins of interest, one annotated as a DyP-type peroxidase family and the other as a peroxidase family 2, herein referred to as DyP2566 and peroxidase-5153 (Table S1), whereas no laccase- or horseradish peroxidase-like homologs were detected, indicating DyPs as the most plausible endogenous catalysts.

These two candidate enzymes were heterologously expressed and evaluated in vitro for their ability to catalyze the transformation of 6-OH-DoE. Among them, DyP2566 efficiently converted 6-OH-DoE to the corresponding dimeric product, with a conversion of approximately 60% of that achieved by Pae-DyP under the same reaction conditions, whereas peroxidase-5153 did not show detectable activity (Figure 3e, traces ii and iii). To explore the structural basis for the different catalytic activities of Pae-DyP and peroxidase-5153, AlphaFold 3 was used to model their compound I states, followed by molecular docking of 6-OH-DoE into the predicted active sites. The docking analysis revealed distinct substrate-binding orientations in the two enzymes (Figure S14). In Pae-DyP, the indole hydroxyl group of 6-OH-DoE is positioned close to the Fe^{IV}=O center. By contrast, steric constraints imposed by active-site residues in peroxidase-5153 orient the substrate such that the hydroxyl group points away from the Fe^{IV}=O center. These contrasting binding modes suggest that the positioning of the indole hydroxyl group relative to the reactive heme center may be an important determinant of substrate oxidation and radical generation, thereby contributing to the observed difference in catalytic activity.

These results provide direct biochemical evidence that *A. versicolor* encodes a cluster-independent DyP capable of catalyzing 6-OH-DoE dimerization in vitro. Together with the absence of any apparent dimerization enzyme within the notoamide biosynthetic gene cluster, this finding strongly supports DyP2566 as a plausible off-pathway endogenous catalyst for this transformation. While a potential contribution from other genome-encoded oxidoreductases, including cytochrome P450 enzymes or other oxidative catalysts, cannot be formally excluded without genetic validation, further genetic studies will be required to establish the physiological role of DyP2566 in vivo.

Elucidating the Mechanistic Basis of DyP-Catalyzed Dimerization

To elucidate the mechanistic basis of the DyP-catalyzed dimerization, we next performed a series of radical-probing, computational, and substrate-based analyses using Pae-DyP as the model catalyst. On the basis of the dimeric structure of the product, a radical-mediated coupling reaction represents a chemically reasonable scenario for the DyP-catalyzed transformation, in which two oxidatively activated substrate units undergo intermolecular coupling. To probe whether radical intermediates are involved in this process, the reaction was first examined in the presence of commonly used radical scavengers, including 2,2,6,6-tetramethylpiperidine 1-oxide (TEMPO) and butylated hydroxytoluene (BHT). LC–MS analysis did not reveal any detectable TEMPO- or BHT-derived radical adducts, suggesting that the reactive intermediates might be short-lived and thus might not be intercepted by conventional scavengers.

Given the limitations of classical radical traps in enzymatic systems, we therefore employed an alternative approach that has been used in peroxidase–hydrogen peroxide systems to probe the involvement of substrate-centered radicals. Previous studies by Cong and co-workers have shown that radicals generated under peroxidase-catalyzed conditions can react with nitrite to afford characteristic nitration products.[46] When sodium nitrite was introduced into the DyP-mediated reaction system, LC–MS analysis revealed the formation of a nitrated derivative (Figure 4a, trace ii and Figure 4b). The detection of this nitration product provides direct experimental evidence for the generation of free radical intermediates during the DyP-catalyzed transformation.

With the involvement of radical species thus established, we next sought to elucidate the origin of the reactive radical by quantum chemical calculations. Bond dissociation energy (BDE) analysis was performed for all potentially abstractable C–H bonds on the indole ring, as well as for the O–H bond of the indole hydroxyl group (Figure 4c). Notably, homolytic cleavage of the O–H bond was found to be energetically most favorable and was taken as the reference (ΔE = 0.0 kcal/mol), whereas abstraction of any indole C–H bond required substantially higher energies ($\Delta E \approx$ 32–36 kcal/mol). These results indicate that initial oxidation under DyP/H_2O_2 conditions preferentially generates an O-centered radical rather than a carbon-centered radical directly on the indole ring. This mechanistic interpretation is also consistent with the docking model of the Pae-DyP–6-OH-DoE complex, in which the

Downloaded from pubs.acs.org/acscatal/article-pdf/doi/10.1021/acscatal.6c03866/6740955O/cs-2026-03866s.pdf?guestAccessKey=b21ef2db-9291-4e47-bb75-c7f3ccfbad6a by guest on 26 August 2026

https://doi.org/10.1021/acscatal.6c03866
ACS Catal. XXXX, XXX, XXX–XXX

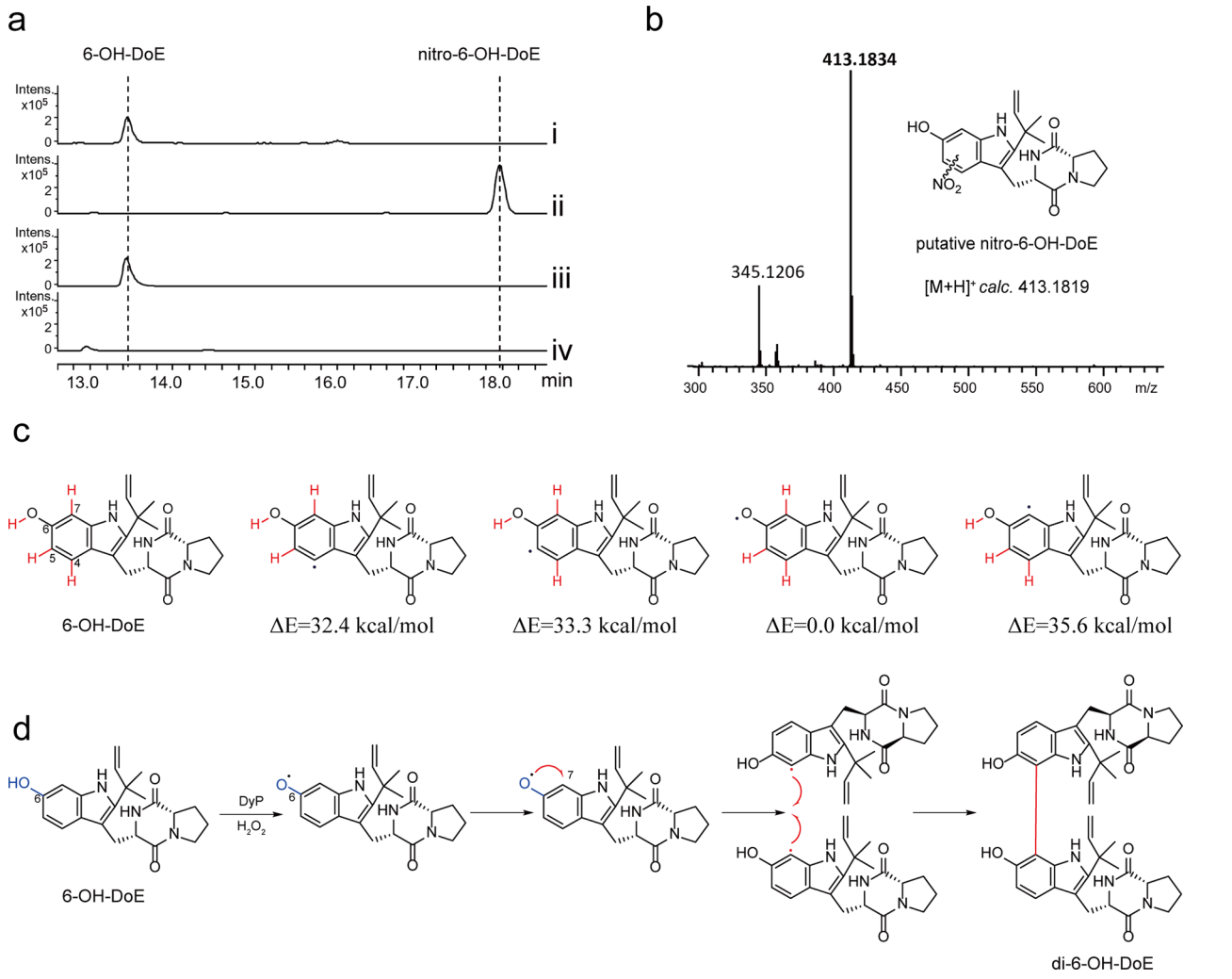

Figure 4. Computational and mechanistic analysis of DyP-catalyzed dimerization of 6-OH-DoE. (a) Extracted ion chromatogram (EIC) analysis from LC-MS results of free radical capture reactions. (i) Control using boiled DyP with the introduction of sodium nitrite; (ii) reaction of the active DyP with the introduction of sodium nitrite; (iii) reaction of the boiled DyP without the addition of sodium nitrite; (iv) reaction with the active DyP without the introduction of sodium nitrite. (b) HRESIMS data analysis of the target nitrated product, nitro-6-OH-DoE. (c) Calculated BDEs for homolytic cleavage of the indole O–H bond and representative indole C–H bonds in 6-OH-DoE. The O–H bond shows the lowest dissociation energy (ΔE = 0.0 kcal/mol, set as the reference), whereas abstraction of indole C–H bonds requires substantially higher energies ($\Delta E \approx$ 32–36 kcal/mol), consistent with preferential formation of an O-centered radical. (d) Proposed hydroxyl-to-carbon radical relay mechanism for DyP-catalyzed dimerization of 6-OH-DoE, highlighting the initial O-centered radical formation, relay of radical character to C7, and subsequent intermolecular coupling leading to di-6-OH-DoE. Unless otherwise indicated, Pae-DyP was used as the catalyst in all reactions shown.

indole hydroxyl group is oriented toward the reactive Fe^{IV}=O center (Figure S14), providing a favorable binding geometry for its initial oxidation. On the basis of this result, we reasoned that the O-centered radical could undergo intramolecular spin delocalization, enabling redistribution of radical character to the adjacent C7 position of the indole ring (Figure 4d). Formation of a C7-centered radical provides a chemically plausible intermediate that is well positioned for intermolecular C–C bond formation. Subsequent coupling of two such C7-centered radical species rationalizes the observed regioselective C7–C7′ dimerization, ultimately leading to the formation of di-6-OH-DoE. Together, these results support a hydroxyl-to-carbon radical relay model in which DyP-mediated O–H oxidation generates an O-centered radical that relays radical character to the indole carbon framework prior to intermolecular coupling. Consistent with this mechanistic proposal, related radical-mediated C–C bond-forming pathways have been reported in cytochrome P450-catalyzed systems.[47,48] In CYP121-catalyzed biaryl formation, hydrogen-atom abstraction from a phenolic hydroxyl group has been proposed to generate an O-centered radical, followed by redistribution of radical character to the aromatic carbon framework and subsequent intramolecular C–C bond formation.[47] This precedent supports the chemical feasibility of hydroxyl-initiated radical generation and radical-mediated C–C coupling, while also highlighting the distinct catalytic context of the present DyP-catalyzed intermolecular dimerization.

To experimentally test this mechanistic hypothesis, we next examined the role of the indole hydroxyl group using a structural analog. Unlike 6-OH-DoE, DoE lacks an indole hydroxyl group. Thus, DoE was used as the substrate for DyP-catalyzed reactions under otherwise identical conditions. This compound was obtained from the heterologous biosynthetic system as

https://doi.org/10.1021/acscatal.6c03866
ACS Catal. XXXX, XXX, XXX–XXX

Downloaded from pubs.acs.org/acscatal/article-pdf/doi/10.1021/acscatal.6c03866/6740955O/cs-2026-03866s.pdf?guestAccessKey=b21ef2db-9291-4e47-bb75-c7f3cdbad6a by guest on 26 August 2026

described above (Figure 2). When DoE was subjected to identical DyP-catalyzed conditions, no detectable conversion was observed (Figure 5a), underscoring the essential role of the indole hydroxyl group in enabling the transformation.

To further exclude the possibility that the loss of reactivity might arise from steric perturbations rather than chemical functionality, halogenated analogues were rationally designed and investigated. Specifically, Cl and Br substituents were intentionally selected to replace the indole hydroxyl group, as they provide comparable steric occupancy at the corresponding position while eliminating the possibility of oxidative radical formation. On this basis, 6-Cl- and 6-Br-substituted brevianamide F were chemically synthesized and structurally confirmed by NMR spectroscopy (Figure 5b; S10–S13), and were subsequently converted to the corresponding DoE analogues using the prenyltransferase NotF (Figure 5c,d,f,g and Figure S15). Consistent with our proposed mechanistic rationale, when these halogenated analogues were subjected to DyP/H_2O_2 conditions, no dimerization or other detectable transformation was observed (Figure 5e,h). Together, these results demonstrate that replacement of the indole hydroxyl group with sterically comparable but redox-inactive halogen substituents selectively abolishes DyP-catalyzed reactivity, mechanistically establishing the indole hydroxyl group as a key enabling feature for the radical-mediated dimerization.

To further substantiate this mechanistic requirement, a series of indole analogues (**1**–**6**) bearing hydroxyl substituents on the indole ring at different positions were subsequently examined (Figure 6a). Several C6-hydroxylated analogues (**1**, **4**, **5**, and **6**) were found to undergo DyP-catalyzed dimerization in a manner consistent with the proposed mechanism (Figure 6b trace ii; Figure 6e trace ii; Figure 6f trace ii; Figure 6g trace ii). When substrates **2** and **3** bearing hydroxyl groups at the C7 or C5 positions of the indole ring were examined, HPLC-HRMS analysis revealed that these substrates were likewise competent for DyP-catalyzed dimerization, affording dimeric products under identical reaction conditions (Figure 6c trace ii; Figure 6d trace ii). Because these dimeric products were generated in amounts insufficient for preparative isolation and comprehensive NMR characterization, their precise coupling positions could not be established in the present study. Future isolation and structural characterization of the dimeric products derived from substrates **2** and **3** will be important for determining how relocation of the indole hydroxyl group from C6 to C7 or C5 reshapes the preferred coupling site and regioselectivity of DyP-catalyzed dimerization. When considered together with the results obtained from structurally modified substrates lacking a hydroxyl group

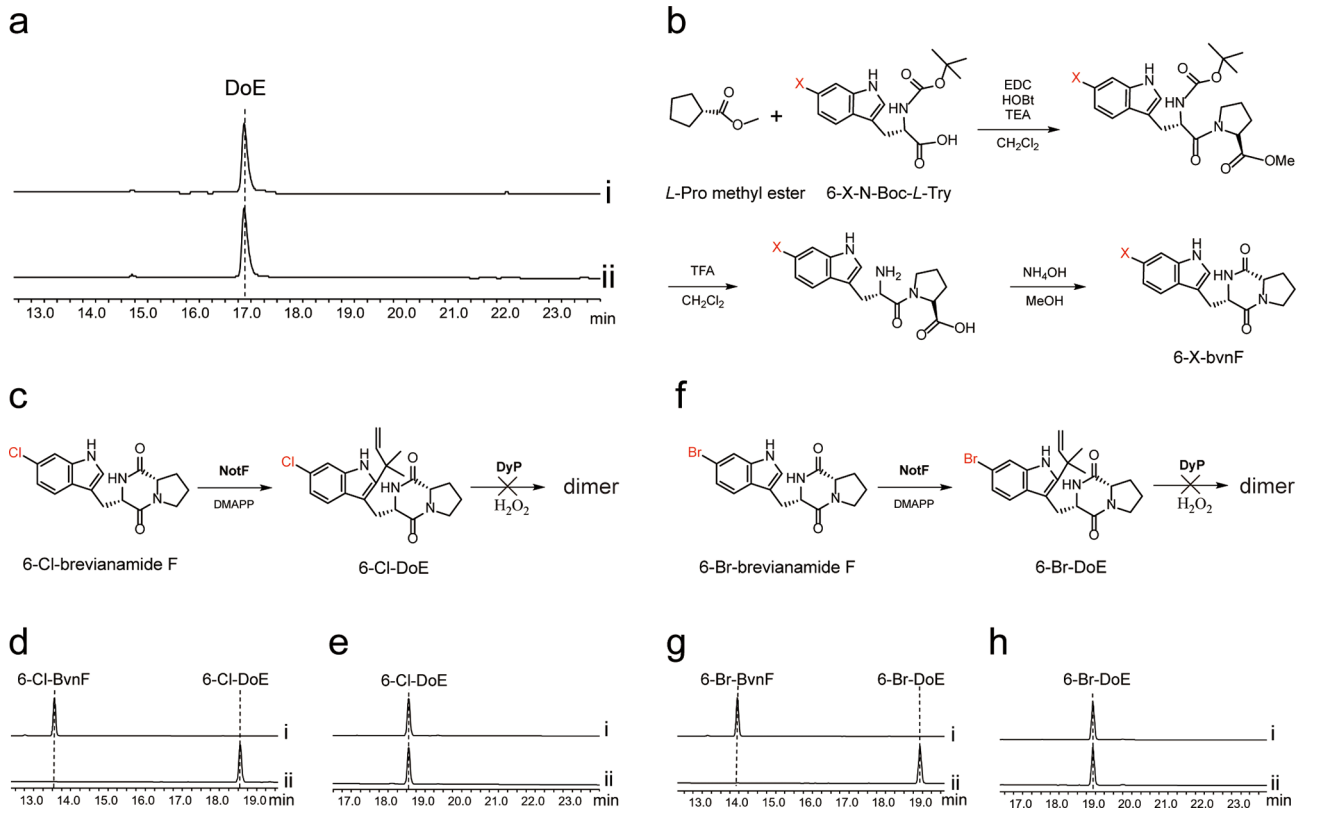

Figure 5. Investigating the proposed mechanism with halogen-substituted substrates. (a) HPLC analysis of the DyP-catalyzed reaction with DoE as the substrate. (i) Control with boiled DyP and (ii) the reaction with the active DyP. (b) Schematic diagram of chemical synthesis of halogen-substituted substrates, 6-X-brevianamide F (6-X-bvnF); "X" indicates Cl or Br. (c) Design of a cascade in vitro reaction with the Cl-substituted substrate, 6-Cl-brevianamide F (6-Cl-bvnF). (d) HPLC analysis of the NotF-catalyzed reaction of 6-Cl-bvnF with 2 mM DMAPP and 100 mM potassium phosphate (pH 7.0); (i) control with boiled NotF; (ii) reaction with the active NotF. (e) HPLC analysis of the DyP-catalyzed reaction of 6-Cl-DoE; (i) control with boiled DyP; (ii) reaction with the active DyP. (f) Design of a cascade reaction with the bromine-substituted substrate, 6-Br-brevianamide F (6-Br-bvnF). (g) HPLC analysis of the NotF-catalyzed reaction of 6-Br-bvnF; (i) control with boiled NotF; (ii) reaction with the active NotF. (h) HPLC analysis of the DyP-catalyzed reaction of 6-Br-DoE; (i) control with boiled DyP; (ii) reaction with the active DyP. Unless otherwise indicated, Pae-DyP was used as the catalyst in all reactions shown.

Downloaded from pubs.acs.org/acscatsci/article-pdf/doi/10.1021/acscatal.6c03866/6740955O/cs-2026-03866s.pdf?guestAccessKey=b21ef2db-9291-4e47-bb75-c7f3cdbad6a by guest on 26 August 2026

https://doi.org/10.1021/acscatal.6c03866
ACS Catal. XXXX, XXX, XXX–XXX

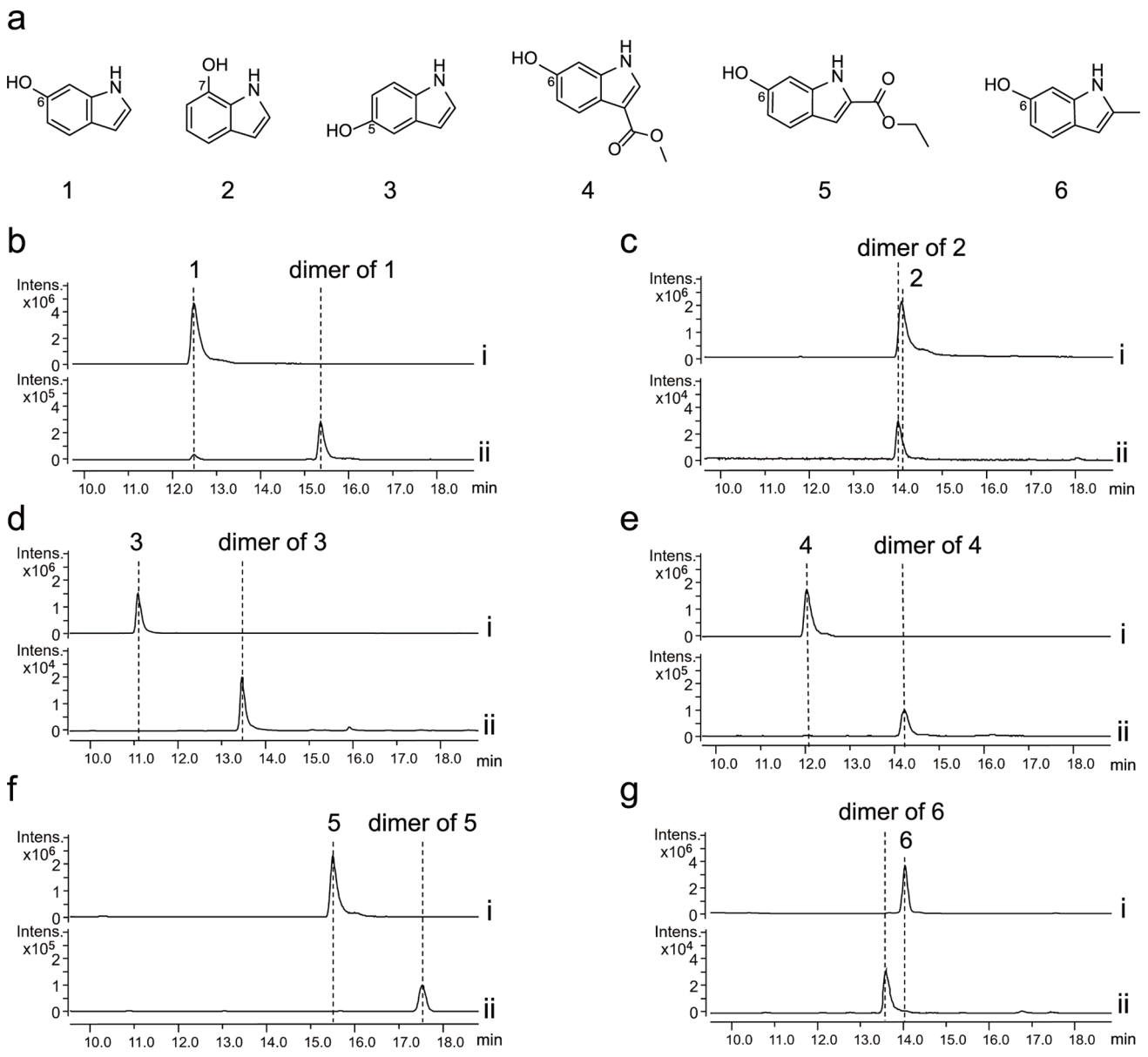

Figure 6. Mechanistic validation of DyP-catalyzed dimerization using hydroxylated indole substrate analogues. (a) Structures of the hydroxylated indole substrate analogues. (b–g) EICs from HPLC-HRMS analyses of DyP-catalyzed reactions using indole analogues **1–6**, respectively. For each substrate, the corresponding control reaction (trace i) using heat-inactivated DyP and the reaction (trace ii) with active DyP are shown. Approximate product yields, estimated from the ratio of the EIC peak area of each dimeric product to that of the corresponding substrate, were 6.2% (b), 0.7% (c), 1.3% (d), 5.5% (e), 4.2% (f), and 0.9% (g) for substrates **1–6**, respectively. The total ion chromatograms (TICs) for the reactions with active DyP are provided in Figures S16–S21. Unless otherwise indicated, Pae-DyP was used as the catalyst in all reactions shown.

or bearing halogen substitutions at the corresponding position, these observations support the conclusion that the indole hydroxyl group is a decisive structural element for this transformation. Taken together, we conclude that the mechanism involves oxidation of the indole hydroxyl group, which initiates substrate-centered radical formation, ultimately enabling regioselective intermolecular coupling in the DyP-catalyzed dimerization reaction (Figure 4d).

■ CONCLUSIONS

In summary, we have elucidated the enzymatic basis and mechanistic principles underlying the dimerization of the indole DKP alkaloid intermediate 6-OH-DoE. Through systematic screening of oxidoreductases, DyPs were identified as effective catalysts for this transformation, and both bacterial and native fungal DyP-type peroxidases were shown to catalyze the regioselective C7–C7′ dimerization. These findings provide a biochemical explanation for the formation of naturally occurring dimeric derivatives of 6-OH-DoE and suggest that such transformations should be mediated by cluster-independent oxidative enzymes in the native producer.

Mechanistic investigations combining radical-probing experiments, quantum chemical calculations, and substrate-based structure–reactivity analysis revealed that dimerization proceeds through a hydroxyl-to-carbon radical relay mechanism, in which

Downloaded from pubs.acs.org/acscatal/article-pdf/doi/10.1021/acscatal.6c03866/6740955O/cs-2026-03866s.pdf?guestAccessKey=b21ef2db-9291-4e47-bb75-c7f3cdbad6a by guest on 26 August 2026

https://doi.org/10.1021/acscatal.6c03866
ACS Catal. XXXX, XXX, XXX–XXX

oxidation of the indole hydroxyl group generates an O-centered radical that subsequently undergoes intramolecular redistribution to a carbon-centered radical. BDE analysis indicates that O–H bond cleavage is energetically favored over direct C–H abstraction, rationalizing the preferential formation of an O-centered radical followed by relay of radical character to the C7 position. The essential role of the indole hydroxyl group was further established by the complete loss of reactivity observed for substrates lacking this functionality or bearing redox-inactive halogen substitutions, as well as by the competence of multiple hydroxylated indole analogues to undergo DyP-catalyzed dimerization.

These results define a coherent mechanistic framework for DyP-catalyzed indole DKP dimerization and highlight the indole hydroxyl group as a key chemical trigger for radical initiation and regioselective intermolecular coupling. More broadly, this study expands the known catalytic repertoire of DyPs in natural product biosynthesis and underscores the potential role of promiscuous oxidative enzymes in generating structural complexity beyond biosynthetic gene clusters.

METHODS

Strains and Culture Conditions

The *E. coli* DH5α strain was used for vector construction and plasmid isolation and was grown on Luria-Bertani (LB) agar plates or LB broth. The *E. coli* BL21(DE3) strain was selected as the host for heterologous protein expression and purification (unless otherwise stated) and was cultured in LB broth or Terrific Broth (TB, 1.2% tryptone, 2.4% yeast extract, 0.94% K_2HPO_4, 0.22% KH_2PO_4, 4% glycerol). Unless otherwise specified, all the *E. coli* strains were cultured at 37 °C, with appropriate antibiotics added to the culture media. *Pichia pastoris* GS115 was used as the host for heterologous protein production and purification of the Jed peroxidase (which failed to achieve soluble protein production when using *E. coli* strains for this protein expression). The culture conditions of *Pichia pastoris* GS115 followed the previous report.[49]

The *Ao* strain was obtained from the storage collection of our laboratory and was used as the host strain for heterologously expressing the cascade enzymes from the notoamide biosynthetic pathway. The *Ao* strains were grown on DPY (2% dextrin, 1% polypeptone, 0.5% yeast extract, 2% agar) agar plates at 30 °C for 7 days. To produce and harvest the target metabolites on a large scale, the *Ao* transformants were picked and cultured in CMOA (Czapek-Dox broth, 3% maltose, 0.1% ornithine, 0.1% ATP) liquid medium at 28 °C with shaking at 200 rpm for 5–10 days.

Protein Expression and Purification

Initially, a single colony of *E. coli* BL21(DE3) carrying the plasmid expressing the target heterologous enzyme was picked from the culturing agar plates; and then it was inoculated into 5 mL LB broth with appropriate antibiotics and incubated at 37 °C for 12 h (overnight). The overnight seed culture was inoculated into 500 mL of TB broth at a ratio of 1:100. When the OD_{600} reached 0.6–1.0, the expression of protein was induced by the addition of isopropyl-β-D-thiogalactoside (IPTG) with a final concentration of 0.2 mM. After incubation at 16–18 °C for 18–20 h, the induced cells were harvested by centrifugation at 4 °C (5000 × *g*, 20 min) and then stored at −80 °C for at least 30 min before being thawed at room temperature for subsequent protein purification. Alternatively, the cell pellet could be stored at −80 °C until later use.

The whole process for protein purification was performed at 4 °C. In brief, 40 mL of cold lysis buffer (50 mM NaH_2PO_4, 300 mM NaCl, 10% glycerol, 10 mM imidazole, pH 8.0) was used to resuspend the cell pellet by vortexing. Following ultrasonication (5 s on, 10 s off, 40 min) using a Model 500 Sonic Dismembrator, the crude cell lysate was centrifuged at 12,000 × *g* at 4 °C for 1 h. Then, the supernatant was collected and mixed with 1 mL of Ni-NTA resin (Qiagen, Hilden, Germany) pre-equilibrated with lysis buffer before use. After incubation at 4 °C for 30 min on a gentle rotator, the slurry was transferred to an empty column. The resin with bound target proteins was washed with 100 mL Wash buffer (50 mM NaH_2PO_4, 300 mM NaCl, 10% glycerol, 20 mM imidazole, pH 8.0) until no noticeable protein in the flow-through could be detected by the Coomassie Brilliant Blue G250 assay. Next, the resin was eluted with about 10 mL of Elution buffer (50 mM NaH_2PO_4, 300 mM NaCl, 10% glycerol, 250 mM imidazole, pH 8.0) (until no noticeable protein was detected with the same G250 assay). The eluate was collected and concentrated to about 2 mL using an Amicon Ultra centrifugal filter concentrator (Merck KGaA, Darmstadt, Germany) by centrifugation at 5000 × *g* at 4 °C, and then the concentrated protein solution underwent buffer-exchange with desalting buffer (50 mM NaH_2PO_4, 10% glycerol). After buffer-exchanging, the final protein fraction was aliquoted and flash-frozen with liquid nitrogen and stored at −80 °C. Protein concentrations were determined by the Bradford method using BSA as a standard.

In Vitro Enzyme Assays

The in vitro oxidoreductase-catalyzed reactions were performed as described in previous reports with minor alterations.[50,51] In general, the reaction mixture contained 1 mM substrate, 2 mM H_2O_2, and ∼10 μL enzyme solution (final enzyme concentration: 10 μM) in 100 μL potassium phosphate buffer (100 mM, pH 7.0) and was incubated at 30 °C for 2–3 h. The reaction was stopped by adding an equal volume of methanol after incubation. All candidate oxidoreductases for the dimerization reaction were tested with the standard substrate, 2,4-dimethylphenol (DMP), to identify the enzymatic activity.

The in vitro NotF-catalyzed reaction was performed in a mixture containing 1 mM substrate, 1 mM DMAPP, 5 mM $MgCl_2$, 10 μL NotF within a total of 100 μL potassium phosphate buffer (100 mM, pH 7.0). For the two-step cascade reaction, the first step of the reaction involved the entire NotF catalytic system with 5 μL of the enzyme. After incubation at 30 °C for 2 h, the second-step reaction for DyP catalysis was triggered by supplementing 5 μL of DyP and 2 μL of H_2O_2 (a final concentration of 2 mM) and incubating the mixture for another 2–3 h. The substrate 6-OH-DoE was also tested in this co-buffer mixture of the two-step reaction, and it was detected to be suitable for the DyP-catalyzed reaction.

Analytical Methods

For monitoring the fermentation and production of the target metabolites of the *Ao* transformants, 1 mL of the culturing mixture was taken from each fermentation flask daily (from the 3rd day until the end of the fermentation). The metabolites were extracted with ethyl acetate and dissolved in methanol and were then analyzed by HPLC. For analysis of the in vitro assays, an equal volume of methanol was added to each reaction mixture to stop the reaction and precipitate the enzymes; after a 20-min denaturation process and 10-min centrifugation at the maximum speed, the supernatant was collected for HPLC analysis.

For HPLC analysis, all samples were analyzed on an Agilent 1260 system with a photodiode array detector. Compound separation was performed on a YMC Triart-C18 column (250 × 4.6 mm, 5 μm) using a linear mobile phase gradient with water (containing 0.1% v/v TFA) and acetonitrile as the solvent system. The detailed linear gradient program was as follows: 0–1 min, 10% acetonitrile; 1–26 min, 10–100% linear gradient of acetonitrile; 26–30 min, 100% acetonitrile; 30–31 min, 100–10% linear gradient of acetonitrile; 31–35 min, 10% acetonitrile. The flow rate was set at 1 mL/min, and the injection volume was 10 μL. The detection wavelength for target compounds was set at 254 nm, and full-wavelength scans (210–400 nm) were also recorded.

Downloaded from pubs.acs.org/acscatal/article-pdf/doi/10.1021/acscatal.6c03866/6740955O/cs-2026-03866s.pdf?guestAccessKey=b21ef2db-9291-4e47-bb75-c7f3cdbad6a by guest on 26 August 2026

https://doi.org/10.1021/acscatal.6c03866
ACS Catal. XXXX, XXX, XXX–XXX

Transformation in *Aspergillus oryzae* M-2-3 (*Ao*)

A spore suspension of *Ao* was inoculated into DPY medium (2% dextrin, 1% polypeptone, 0.5% yeast extract). After incubation at 30 °C with shaking at 200 rpm for about 3 days, the mycelia were harvested by filtration and washed with ddH_2O. The protoplasts were prepared by digestion with Yatalase (Takara, 5.0 mg/mL) in Solution I (0.8 M NaCl, 10 mM NaH_2PO_4, pH 8.0) at 30 °C for 2 hours. After centrifugation at 2500 × *g* for 5 min, the protoplasts were washed with 0.8 M sterilized NaCl solution. Next, the protoplasts were adjusted to about 2.0×10^8 cells per mL by adding Solution II (0.8 M NaCl, 10 mM $CaCl_2$, and 10 mM Tris–HCl, pH 8.0) and Solution III (40% (w/v) PEG4000, 50 mM $CaCl_2$, 50 mM Tris–HCl, pH 8.0) at a ratio of 4:1. For single transformation, the appropriate plasmid (about 10 μg) was added to the protoplast solution (200 μL) with gentle mixing. Following incubation on ice for 20 min, 1 mL of Solution III was added to the protoplast solution. After another 20 min of incubation at room temperature, the transformation mixture was mixed with pre-melted (at 45 °C) soft-top agar medium (1.2 M sorbitol, 3.5% CD broth, 0.6% agar) and immediately poured onto CD agar plates supplemented with 1 M sorbitol. After the soft-top agar had completely solidified, the plates were incubated at 30 °C for 7–10 days until colonies appeared.

Synthesis of Halogenated Substrates

The synthesis of halogenated substrates was carried out according to the previous report.[22] In brief, the synthesis comprised three steps. Step 1: at 0 °C, triethylamine (TEA, 4.5 equiv) was added dropwise to a solution of L-Pro methyl ester hydrochloride (1.0 equiv) in 0.1 M CH_2Cl_2; 1-hydroxybenzotriazole hydrate (HOBt·H_2O, 1.5 equiv) and 6-X-N-Boc-L-tryptophan (1.5 equiv) were added and agitated strongly (here, X represents Br or Cl); once homogeneous, EDC·HCl (1.5 equiv) was added to the solution. The whole mixture was then warmed to 23 °C; after stirring at 23 °C for 15 h, it was quenched by the addition of 1 M HCl, and the aqueous layer was extracted with CH_2Cl_2 (2×). Step 2: the merged organics were then washed with saturated aqueous $NaHCO_3$, and the aqueous layer was extracted with CH_2Cl_2 (2×) again; the organics were collected and dried with Na_2SO_4; followed by filtration, they were concentrated under vacuum and the resulting oil/foam was repeatedly dissolved in CH_2Cl_2 (0.2 M), and cooled to 0 °C; TFA (3:10 in CH_2Cl_2) was added dropwise, and the mixture was kept at 23 °C. Step 3: following stirring at 23 °C for 2 h, the mixture was condensed under vacuum, and the resulting sticky residue was dissolved in methanol (0.25 M) and cooled to 0 °C; ammonium hydroxide (28–30% in H_2O, 1:6 in MeOH) was added dropwise, and then the whole mixture was set to 23 °C with stirring for 24 h; the resultant suspension was cooled to 0 °C again, and the fine white deposit was filtered and dissolved in cold methanol.

Computational Methods

All quantum chemical calculations were conducted using the Gaussian 16 software package, employing the B3LYP-D3(BJ) functional.[52−56] Geometry optimizations were performed using the 6-31+G(d,p) basis set. The frequency calculations were subsequently carried out at the same theoretical level to obtain thermal corrections for the Gibbs free energies. Based on the optimized structures, single-point energy calculations were executed using the larger 6-311+G(2d,2p) basis set to obtain more accurate energies. The final reported energies correspond to the B3LYP-D3(BJ)/6-311+G(2d,2p) single-point values, corrected for the Gibbs free energies.

BDEs, which are reliable descriptors of bond strength,[57−59] were calculated to identify the most favorable dehydrogenation site in the target compounds (6-hydroxydeoxybrevianamide E). The BDE for a bond A–B is defined as the standard enthalpy change for the homolytic bond cleavage reaction:

$$AB \rightarrow A^{\cdot} + B^{\cdot} \quad (1)$$

expressed numerically as

$$E(AB) = H(A^{\cdot}) + H(B^{\cdot}) - H(AB) \quad (2)$$

where $E(AB)$ is the BDE, $H(A^{\cdot})$, $H(B^{\cdot})$, and $H(AB)$ are the enthalpies of formation of radicals $A^{\cdot}$, $B^{\cdot}$, and compound AB.

Structure Prediction and Molecular Docking

The three-dimensional structures of Pae-DyP and peroxidase-5153 in complex with the heme cofactor (HEM) were generated using AlphaFold 3.[60] To computationally mimic the catalytically active species, HEM was subsequently converted to compound I (Cpd I) by manually adding an oxo ligand to the heme iron, forming the characteristic Fe^{IV}=O moiety. Molecular docking simulations were performed using AutoDock (v4.2.6) [61] to investigate the potential binding modes of 6-OH-DoE within the enzyme–Cpd I complexes. During receptor preparation, water molecules were removed from the macromolecule, and polar hydrogens and Kollman charges were assigned to the enzyme–Cpd I complex. Both the prepared protein and ligand were saved in .pdbqt format. The docking grid was centered on the Cpd I-binding pocket with grid dimensions of 40 × 40 × 40. AutoGrid was executed using the corresponding .pdbqt files. Docking simulations were conducted using the Lamarckian Genetic Algorithm (LGA), with a total of 500 docking runs performed per system to ensure a comprehensive exploration of the conformational binding space.

■ ASSOCIATED CONTENT

Supporting Information

The Supporting Information is available free of charge at https://pubs.acs.org/doi/10.1021/acscatal.6c03866.

HRMS data; ^{1}H-NMR spectra and ^{13}C-NMR spectra; and total ion chromatograms and amino acid sequences of other proteins (PDF)

■ AUTHOR INFORMATION

Corresponding Authors

Xiang Sheng – *State Key Laboratory of Engineering Biology for Low-Carbon Manufacturing, Tianjin Institute of Industrial Biotechnology, Chinese Academy of Sciences, Tianjin 300308, China; National Technology Innovation Center for Synthetic Biology, Tianjin 300308, China;* orcid.org/0000-0002-6542-6649; Email: shengx@tib.cas.cn

Lei Du – *State Key Laboratory of Microbial Technology, Shandong University, Qingdao, Shandong 266237, China; National Key Laboratory of Agricultural Microbiology, College of Life Science and Technology, Hubei Hongshan Laboratory, Huazhong Agricultural University, Wuhan 430070, China;* orcid.org/0000-0003-2245-7100; Email: lei.du@sdu.edu.cn

Shengying Li – *State Key Laboratory of Microbial Technology, Shandong University, Qingdao, Shandong 266237, China; Laboratory for Marine Biology and Biotechnology, Qingdao Marine Science and Technology Center, Qingdao, Shandong 266237, China;* orcid.org/0000-0002-5244-870X; Email: lishengying@sdu.edu.cn

Authors

Peng Fang – *State Key Laboratory of Microbial Technology, Shandong University, Qingdao, Shandong 266237, China*

Wei Wang – *State Key Laboratory of Engineering Biology for Low-Carbon Manufacturing, Tianjin Institute of Industrial Biotechnology, Chinese Academy of Sciences, Tianjin 300308,*

Downloaded from pubs.acs.org/acscatal/article-pdf/doi/10.1021/acscatal.6c03866/6740950/cs-2026-03866s.pdf?guestAccessKey=b21cf2db-9291-4e47-bb75-c7f3cdbad6a by guest on 26 August 2026

China; National Technology Innovation Center for Synthetic Biology, Tianjin 300308, China
Shuai Mu – *Tianjin Institute of Pharmaceutical Research, Tianjin 300193, China*
Fei Guo – *State Key Laboratory of Microbial Technology, Shandong University, Qingdao, Shandong 266237, China*
Xinwei Song – *State Key Laboratory of Microbial Technology, Shandong University, Qingdao, Shandong 266237, China*

Complete contact information is available at: https://pubs.acs.org/doi/10.1021/acscatal.6c03866

Author Contributions

P.F. conducted investigation, formal analysis, and methodology and wrote the original draft of the manuscript. W.W. carried out investigation, formal analysis, and methodology and participated in manuscript drafting. S.M. performed validation, investigation, and data curation. F.G. completed investigation, validation, and data curation. Xinwei S. undertook investigation, data curation, and validation. Xiang S. was involved in conceptualization and methodology and revised and edited the manuscript. L.D. engaged in conceptualization, supervision, formal analysis, and funding acquisition and assisted with manuscript revision and editing. S.L., as the corresponding author, took charge of conceptualization, supervision, formal analysis, and funding acquisition and finalized the manuscript review and editing. All authors read and approved the final version of the manuscript.

Notes

The authors declare no competing financial interest.

■ ACKNOWLEDGMENTS

This research was supported by the National Key Research and Development Program of China (2025YFD1700400, 2021YFA0911500), the National Natural Science Foundation of China (32370032, 22237004), the Taishan Young Scholars (tsqn202312032), the Key R&D Program of Shandong Province (2025CXPT190), and the Fundamental Research Funds of Shandong University (2023QNTD001). The authors acknowledge Shandong University Core Facilities for Life and Environmental Sciences for their help with LC-MS and NMR.

■ REFERENCES

(1) Ma, Y.; Liang, X.; Kong, Y.; Jia, B. Structural diversity and biological activities of indole diketopiperazine alkaloids from fungi. *J. Agric. Food Chem.* **2016**, *64* (35), 6659–6671.
(2) Yang, J.; Gong, L.; Guo, M.; Jiang, Y.; Ding, Y.; Wang, Z.; Xin, X.; An, F. Bioactive indole diketopiperazine alkaloids from the marine endophytic fungus *Aspergillus* sp YJ191021. *Mar. Drugs* **2021**, *19* (3), 157.
(3) Yan, L.; Du, F.; Li, X.; Yang, S.; Wang, B.; Li, X. Antibacterial indole diketopiperazine alkaloids from the deep-sea cold seep-derived fungus *Aspergillus chevalieri*. *Mar. Drugs* **2023**, *21* (3), 195.
(4) Zhang, Y.; Geng, C.; Zhang, X.; Zhu, H.; Shao, C.; Cao, F.; Wang, C. Discovery of bioactive indole-diketopiperazines from the marine-derived fungus *Penicillium brasilianum* aided by genomic information. *Mar. Drugs* **2019**, *17* (9), 514.
(5) Huo, R.; Zhang, J.; Niu, S.; Liu, L. New prenylated indole diketopiperazine alkaloids and polyketides from the mangrove-derived fungus *Penicillium* sp. *Front. Mar. Sci.* **2022**, *9*, 1097594.
(6) Wang, F.; Tong, Q.; Ma, H.; Xu, H.; Hu, S.; Ma, W.; Xue, Y.; Liu, J.; Wang, J.; Song, H.; Zhang, J.; Zhang, G.; Zhang, Y. Indole diketopiperazines from endophytic *Chaetomium sp 88194* induce breast cancer cell apoptotic death. *Sci. Rep.* **2015**, *5* (1), 9294.
(7) Zhang, H.; Sun, C.; Xia, Q.; Li, P.; Liu, K.; Zhang, Y. Brevianamide F exerts antithrombotic effects by modulating the MAPK signaling pathway and coagulation cascade. *Mar. Drugs* **2024**, *22* (10), 439.
(8) Hu, L.; Zhang, T.; Liu, D.; Guan, G.; Huang, J.; Proksch, P.; Chen, X.; Lin, W. Notoamide-type alkaloid induced apoptosis and autophagy via a P38/JNK signaling pathway in hepatocellular carcinoma cells. *RSC Adv.* **2019**, *9* (34), 19855–19868.
(9) Zhao, S.; Smith, K.; Deveau, A.; Dieckhaus, C.; Johnson, M.; Macdonald, T.; Cook, J. Biological activity of the tryprostatins and their diastereomers on human carcinoma cell lines. *J. Med. Chem.* **2002**, *45* (8), 1559–1562.
(10) Ma, Y.; Zhang, H.; Zhao, J.; Li, X. Secondary anti-fungi metabolites from the endophytic fungus *Fusarium* sp in *Eucommia ulmoides*. *Chem. Nat. Compd.* **2012**, *48* (1), 170–171.
(11) Cui, C.; Kakeya, H.; Osada, H. Spirotryprostatin B, a novel mammalian cell cycle inhibitor produced by *Aspergillus fumigatus*. *J. Antibiot.* **1996**, *49* (8), 832–835.
(12) Wulff, J.; Siegrist, R.; Myers, A. The natural product avrainvillamide binds to the oncoprotein nucleophosmin. *J. Am. Chem. Soc.* **2007**, *129* (46), 14444–14451.
(13) Li, P.; Zhang, M.; Li, H.; Wang, R.; Hou, H.; Li, X.; Liu, K.; Chen, H. New prenylated indole homodimeric and pteridine alkaloids from the marine-derived fungus *Aspergillus austroafricanus* Y32-2. *Mar. Drugs* **2021**, *19* (2), 98.
(14) Ola, A.; Debbab, A.; Aly, A.; Mandi, A.; Zerfass, I.; Hamacher, A.; Kassack, M.; Brötz-Oesterhelt, H.; Kurtan, T.; Proksch, P. Absolute configuration and antibiotic activity of neosartorin from the endophytic fungus *Aspergillus fumigatiaffinis*. *Tetrahedron Lett.* **2014**, *55* (5), 1020–1023.
(15) Gilbert, N.; O'Reilly, J.; Chang, C.; Lin, Y.; Brueggemeier, R. Antiproliferative activity of gossypol and gossypolone on human breast cancer cells. *Life Sci.* **1995**, *57* (1), 61–67.
(16) Qian-Cutrone, J.; Huang, S.; Shu, Y.; Vyas, D.; Fairchild, C.; Menendez, A.; Krampitz, K.; Dalterio, R.; Klohr, S.; Gao, Q. Stephacidin A and B: two structurally novel, selective inhibitors of the testosterone-dependent prostate LNCaP cells. *J. Am. Chem. Soc.* **2002**, *124* (49), 14556–14557.
(17) Guo, Z.; Li, P.; Chen, G.; Li, C.; Cao, Z.; Zhang, Y.; Ren, J.; Xiang, H.; Lin, S.; Ju, J.; Chen, Y. Design and biosynthesis of dimeric alboflavusins with biaryl linkages via regiospecific C–C bond coupling. *J. Am. Chem. Soc.* **2018**, *140* (51), 18009–18015.
(18) Aruwa, C.; Amoo, S.; Koorbanally, N.; Kudanga, T. Enzymatic dimerization of luteolin enhances antioxidant and antimicrobial activities. *Biocatal. Agric. Biotechnol.* **2021**, *35*, 102105.
(19) Lorenzon, E.; Piccoli, J.; Santos-Filho, N.; Cilli, E. Dimerization of antimicrobial peptides: a promising strategy to enhance antimicrobial peptide activity. *Protein Pept. Lett.* **2019**, *26* (2), 98–107.
(20) Drapier, T.; Geubelle, P.; Bouckaert, C.; Nielsen, L.; Laulumaa, S.; Goffin, E.; Dilly, S.; Francotte, P.; Hanson, J.; Pochet, L.; Kastrup, J.; Pirotte, B. Enhancing action of positive allosteric modulators through the design of dimeric compounds. *J. Med. Chem.* **2018**, *61* (12), 5279–5291.
(21) Saruwatari, T.; Yagishita, F.; Mino, T.; Noguchi, H.; Hotta, K.; Watanabe, K. Cytochrome P450 as Dimerization Catalyst in Diketopiperazine Alkaloid Biosynthesis. *ChemBioChem* **2014**, *15* (5), 656–659.
(22) Tian, W.; Sun, C.; Zheng, M.; Harmer, J.; Yu, M.; Zhang, Y.; Peng, H.; Zhu, D.; Deng, Z.; Chen, S.; Mobli, M.; Jia, X.; Qu, X. Efficient biosynthesis of heterodimeric C3-aryl pyrroloindoline alkaloids. *Nat. Commun.* **2018**, *9* (1), 4428.
(23) Shende, V. V.; Khatri, Y.; Newmister, S. A.; Sanders, J. N.; Lindovska, P.; Yu, F.; Doyon, T. J.; Kim, J.; Houk, K. N.; Movassaghi, M.; Sherman, D. H. Structure and Function of NzeB, a Versatile C–C and C–N Bond-Forming Diketopiperazine Dimerase. *J. Am. Chem. Soc.* **2020**, *142* (41), 17413–17424.
(24) Ueda, H.; Sato, S.; Noda, K.; Hakamata, H.; Kwon, E.; Kobayashi, N.; Tokuyama, H. Iron-Catalyzed Biomimetic

Downloaded from pubs.acs.org/acscatal/article-pdf/doi/10.1021/acscatal.6c03866/6740955O/cs-2026-03866s.pdf?guestAccessKey=b21ef2db-9291-4e47-bb75-c7f3cdbad6a by guest on 26 August 2026

Dimerization of Tryptophan-Containing Peptides. *Angew. Chem., Int. Ed.* **2023**, *62* (22), e202302404.
(25) Galeazzi, L.; Ronchi, P.; Franceschi, C.; Giunta, S. In vitro peroxidase oxidation induces stable dimers of beta-amyloid (1-42) through dityrosine bridge formation. *Amyloid* **1999**, *6* (1), 7–13.
(26) Arrieta-Baez, D.; Stark, R. Modeling suberization with peroxidase-catalyzed polymerization of hydroxycinnamic acids: cross-coupling and dimerization reactions. *Phytochemistry* **2006**, *67* (7), 743–753.
(27) Gomi, K.; Iimura, Y.; Hara, S. Integrative transformation of Aspergillus oryzae with a plasmid containing the *Aspergillus nidulans* argB gene. *Agric. Biol. Chem.* **1987**, *51* (9), 2549–2555.
(28) Heneghan, M. N.; Yakasai, A. A.; Halo, L. M.; Song, Z.; Bailey, A. M.; Simpson, T. J.; Cox, R. J.; Lazarus, C. M. First Heterologous Reconstruction of a Complete Functional Fungal Biosynthetic Multigene Cluster. *ChemBioChem* **2010**, *11* (11), 1508–1512.
(29) Li, S.; Anand, K.; Tran, H.; Yu, F.; Finefield, J. M.; Sunderhaus, J. D.; McAfoos, T. J.; Tsukamoto, S.; Williams, R. M.; Sherman, D. H. Comparative analysis of the biosynthetic systems for fungal bicyclo[2.2.2]-diazaoctane indole alkaloids: the (+)/(-)-notoamide, paraherquamide and malbrancheamide pathways. *Medchemcomm* **2012**, *3* (8), 987–996.
(30) Kersten, P. J.; Kalyanaraman, B.; Hammel, K. E.; Reinhammar, B.; Kirk, T. K. Comparison of lignin peroxidase, horseradish peroxidase and laccase in the oxidation of methoxybenzenes. *Biochem. J.* **1990**, *268* (2), 475–480.
(31) Bissaro, B.; Streit, B.; Isaksen, I.; Eijsink, V. G. H.; Beckham, G. T.; DuBois, J. L.; Røhr, Å. K. Molecular mechanism of the chitinolytic peroxygenase reaction. *Proc. Natl. Acad. Sci. U. S. A.* **2020**, *117* (3), 1504–1513.
(32) Guengerich, F.; Yoshimoto, F. Formation and cleavage of C–C bonds by enzymatic oxidation–reduction reactions. *Chem. Rev.* **2018**, *118* (14), 6573–6655.
(33) Long, C.; Cao, H.; Zhao, B.; Tan, Y.; He, Y.; Huang, C.; Guan, Z. Merging the non-natural catalytic activity of lipase and electrosynthesis: asymmetric oxidative cross-coupling of secondary amines with ketones. *Angew. Chem., Int. Ed.* **2022**, *61* (30), e202203666.
(34) Ćirić-Marjanović, G.; Milojević-Rakić, M.; Janošević-Ležaić, A.; Luginbühl, S.; Walde, P. Enzymatic oligomerization and polymerization of arylamines: state of the art and perspectives. *Chem. Pap.* **2017**, *71* (2), 199–242.
(35) Finefield, J.; Sherman, D.; Tsukamoto, S.; Williams, R. Studies on the biosynthesis of the notoamides: synthesis of an isotopomer of 6-hydroxydeoxybrevianamide E and biosynthetic incorporation into notoamide J. *J. Org. Chem.* **2011**, *76* (15), 5954–5958.
(36) Finefield, J.; Kato, H.; Greshock, T.; Sherman, D.; Tsukamoto, S.; Williams, R. Biosynthetic studies of the notoamides: isotopic synthesis of stephacidin A and incorporation into notoamide B and sclerotiamide. *Org. Lett.* **2011**, *13* (15), 3802–3805.
(37) McAfoos, T.; Li, S.; Tsukamoto, S.; Sherman, D.; Williams, R. Studies on the biosynthesis of the stephacidins and notoamides. Total synthesis of notoamide S. *Heterocycles* **2010**, *82* (1), 461–470.
(38) Wan, Y.; Lu, R.; Akiyama, K.; Miyakoshi, T.; Du, Y. Enzymatic synthesis of bioactive compounds by Rhus laccase from Chinese *Rhus vernicifera*. *Sci. China, Ser. B: Chem.* **2007**, *50* (2), 179–182.
(39) Molina-Espeja, P.; Beltran-Nogal, A.; Alfuzzi, M.; Guallar, V.; Alcalde, M. Mapping potential determinants of peroxidative activity in an evolved fungal peroxygenase from *Agrocybe aegerita*. *Front. Bioeng. Biotechnol.* **2021**, *9*, 741282.
(40) van Schijndel, J.; Vollenbroek, E.; Wever, R. The chloroperoxidase from the fungus *Curvularia inaequalis*; a novel vanadium enzyme. *Biochim. Biophys. Acta (BBA)-Protein Struct. Mol. Enzymol.* **1993**, *1161* (2-3), 249–256.
(41) Lavery, C.; Macinnis, M.; Macdonald, M.; Williams, J.; Spencer, C.; Burke, A.; Irwin, D.; D'Cunha, G. Purification of peroxidase from horseradish (*Armoracia rusticana*) roots. *J. Agric. Food Chem.* **2010**, *58* (15), 8471–8476.
(42) Santos, A.; Mendes, S.; Brissos, V.; Martins, L. New dye-decolorizing peroxidases from *Bacillus subtilis* and *Pseudomonas putida* MET94: towards biotechnological applications. *Appl. Microbiol. Biotechnol.* **2014**, *98* (5), 2053–2065.
(43) Park, J.; Lee, S.; Lee, M.; Park, K.; Lee, S.; Kim, J.; Kim, P. Accelerated growth of *Corynebacterium glutamicum* by up-regulating stress-responsive genes based on transcriptome analysis of a fast-doubling evolved strain. *J. Microbiol. Biotechnol.* **2020**, *30* (9), 1420–1429.
(44) Li, J.; Liu, C.; Li, B.; Yuan, H.; Yang, J.; Zheng, B. Identification and molecular characterization of a novel DyP-type peroxidase from *Pseudomonas aeruginosa* PKE117. *Appl. Biochem. Biotechnol.* **2012**, *166* (3), 774–785.
(45) Roberts, J.; Singh, R.; Grigg, J.; Murphy, M.; Bugg, T.; Eltis, L. Characterization of dye-decolorizing peroxidases from *Rhodococcus jostii* RHA1. *Biochemistry* **2011**, *50* (23), 5108–5119.
(46) Wang, X.; Lin, X.; Jiang, Y.; Qin, X.; Ma, N.; Yao, F.; Dong, S.; Liu, C.; Feng, Y.; Jin, L.; Xian, M.; Cong, Z. Engineering cytochrome P450BM3 enzymes for direct nitration of unsaturated hydrocarbons. *Angew. Chem., Int. Ed.* **2023**, *62* (13), e202217678.
(47) Li, S.-H.; Zhang, X.; Mei, Z.-L.; Liu, Y.; Ma, J.-A.; Zhang, F.-G. Chemoenzymatic Synthesis of Fluorinated Mycocyclosin Enabled by the Engineered Cytochrome P450-Catalyzed Biaryl Coupling Reaction. *J. Am. Chem. Soc.* **2024**, *146* (29), 19962–19973.
(48) Yang, E.; Yao, Y.; Su, H.; Sun, Z.; Gao, S.-S.; Sureram, S.; Kittakoop, P.; Fan, K.; Pan, Y.; Xu, X.; Sun, Z.-H.; Ma, G.; Liu, G. Two Cytochrome P450 Enzymes Form the Tricyclic Nested Skeleton of Meroterpenoids by Sequential Oxidative Reactions. *J. Am. Chem. Soc.* **2024**, *146* (16), 11457–11464.
(49) Jiang, X.; Yin, M.; Chen, P.; Yang, Q. Constitutive expression, purification and characterization of bovine prochymosin in *Pichia pastoris* GS115. *World J. Microbiol. Biotechnol.* **2012**, *28* (5), 2087–2093.
(50) Molina-Espeja, P.; Garcia-Ruiz, E.; Gonzalez-Perez, D.; Ullrich, R.; Hofrichter, M.; Alcalde, M. Directed evolution of unspecific peroxygenase from *Agrocybe aegerita*. *Appl. Environ. Microbiol.* **2014**, *80* (11), 3496–3507.
(51) Ghosh, J.; Taylor, K.; Bewtra, J.; Biswas, N. Laccase-catalyzed removal of 2,4-dimethylphenol from synthetic wastewater: effect of polyethylene glycol and dissolved oxygen. *Chemosphere* **2008**, *71* (9), 1709–1717.
(52) Frisch, M. J.; Trucks, G. W.; Schlegel, H. B.; Scuseria, G. E.; Robb, M. A.; Cheeseman, J. R.; Scalmani, G.; Barone, V.; Petersson, G. A.; Nakatsuji, H.; Li, X. Caricato, M.; Marenich, A. V.; Bloino, J.; Janesko, B. G. Gomperts, R.; Mennucci, B.; Hratchian, H. P.; Ortiz, J. V.; Izmaylov, A. F.; Sonnenberg, J. L.; Williams-Young, D.; Ding, F. Lipparini, F.; Egidi, F.; Goings, J. Peng, B.; Petrone, A.; Henderson, T. Ranasinghe, D. Zakrzewski, V. G. Gao, J.; Rega, N.; Zheng, G.; Liang, W.; Hada, M.; Ehara, M. Toyota, K.; Fukuda, R. Hasegawa, J.; Ishida, M.; Nakajima, T.; Honda, Y.; Kitao, O.; Nakai, H.; Vreven, T.; Throssell, K.; Montgomery, J. A., Jr.; Peralta, J. E.; Ogliaro, F.; Bearpark, M. J.; Heyd, J. J.; Brothers, E. N.; Kudin, K. N.; Staroverov, V. N.; Keith, T. A.; Kobayashi, R.; Normand, J. Raghavachari, K.; Rendell, A. P. Burant, J. C.; Iyengar, S. S. Tomasi, J.; Cossi, M.; Millam, J. M.; Klene, M; Adamo, C; Cammi, R.; Ochterski, J. W.; Martin, R. L.; Morokuma, K.; Farkas, O.; Foresman, J. B.; Fox, D. J. *Gaussian 16, Revision C.01,* Gaussian, Inc.Wallingford, CT**2016**
(53) Becke, A. Density-functional thermochemistry. III The role of exact exchange. *J. Chem. Phys.* **1993**, *98* (7), 5648–5652.
(54) Lee, C.; Yang, W.; Parr, R. G. Development of the Colle-Salvetti correlation-energy formula into a functional of the electron density. *Phys. Rev. B* **1988**, *37* (2), 785–789.
(55) Grimme, S.; Antony, J.; Ehrlich, S.; Krieg, H. A consistent and accurate ab initio parametrization of density functional dispersion correction (DFT-D) for the 94 elements H-Pu. *J. Chem. Phys.* **2010**, *132* (15), 154104.
(56) Grimme, S.; Ehrlich, S.; Goerigk, L. Effect of the damping function in dispersion corrected density functional theory. *J. Comput. Chem.* **2011**, *32* (7), 1456–1465.
(57) Feng, Y.; Liu, L.; Wang, J.; Huang, H.; Guo, Q. Assessment of experimental bond dissociation energies using composite ab initio methods and evaluation of the performances of density functional methods in the calculation of bond dissociation energies. *J. Chem. Inf. Comput. Sci.* **2003**, *43* (6), 2005–2013.

Downloaded from pubs.acs.org/acscatal/article-pdf/doi/10.1021/acscatal.6c03866/6740955O/cs-2026-03866s.pdf?guestAccessKey=b21cf2db-9291-4e47-bb75-c7f3ccfbad6a by guest on 26 August 2026

https://doi.org/10.1021/acscatal.6c03866
ACS Catal. XXXX, XXX, XXX–XXX

(58) Izgorodina, E.; Coote, M.; Radom, L. Trends in R–X bond dissociation energies (R= Me, Et, i-Pr, t-Bu; X= H, CH3, OCH3, OH, F): a surprising shortcoming of density functional theory. *J. Phys. Chem. A* **2005**, *109* (33), 7558–7566.
(59) Peng, J.; He, X.; Luo, X.; Zhong, K.; Liao, L.; Bai, R.; Lan, Y. Bond dissociation energy-controlled regioselectivity in hydrofunctionalization. *ACS Catal.* **2024**, *14* (10), 8030–8040.
(60) Abramson, J.; Adler, J.; Dunger, J.; Evans, R.; Green, T.; Pritzel, A.; Ronneberger, O.; Willmore, L.; Ballard, A. J.; Bambrick, J.; Bodenstein, S. W.; Evans, D. A.; Hung, C.-C.; O'Neill, M.; Reiman, D.; Tunyasuvunakool, K.; Wu, Z.; Žemgulytė, A.; Arvaniti, E.; Beattie, C.; Bertolli, O.; Bridgland, A.; Cherepanov, A.; Congreve, M.; Cowen-Rivers, A. I.; Cowie, A.; Figurnov, M.; Fuchs, F. B.; Gladman, H.; Jain, R.; Khan, Y. A.; Low, C. M. R.; Perlin, K.; Potapenko, A.; Savy, P.; Singh, S.; Stecula, A.; Thillaisundaram, A.; Tong, C.; Yakneen, S.; Zhong, E. D.; Zielinski, M.; Žídek, A.; Bapst, V.; Kohli, P.; Jaderberg, M.; Hassabis, D.;Jumper, J. M. Accurate structure prediction of biomolecular interactions with AlphaFold 3. *Nature* **2024**, *630* (8016), 493–500.
(61) Morris, G. M.; Huey, R.; Lindstrom, W.; Sanner, M. F.; Belew, R. K.; Goodsell, D. S.; Olson, A. J. AutoDock4 and AutoDockTools4: Automated docking with selective receptor flexibility. *J. Comput. Chem.* **2009**, *30* (16), 2785–2791.

Downloaded from pubs.acs.org/accacs/article-pdf/doi/10.1021/acscatal.6c03866/6740955O/cs-2026-03866s.pdf?guestAccessKey=b21ef2db-9291-4e47-bb75-c7f3cfbad6a by guest on 26 August 2026

https://doi.org/10.1021/acscatal.6c03866
ACS Catal. XXXX, XXX, XXX–XXX